

for 45 min. Coverslips were mounted together with 4',6-diamidino-2-phenylindole (DAPI, Invitrogen, CA) for nuclear localization, and then visualized under epifluorescence using Axiophoto II (Carl Zeiss).

To detect lysosomal localization, cells were incubated with PBS containing 100 nM of Lyso-Tracker[®] (Invitrogen) at 37°C for 1 hour. After rinsing with PBS, cells were fixed with 4% paraformaldehyde at 37°C for 20 min.

Immunoblotting analysis of LC3. *Lmna*^{H222P/H222P} and wild-type MEF were grown on 100 mm-collagen I coated dishes. At 80% confluent state, cells were treated with lysosomal protease inhibitors consisting of pepstatin A (20 µg/mL, Peptide Institute, Osaka, Japan) and E64d (20 µg/mL, Peptide Institute), or with dimethylsulfoxide (DMSO) as a negative control for 4 hours. Whole cell lysates was extracted with lysis buffer (1% NP-40 cell lysis buffer supplemented with protease inhibitor). Immunoblotting analysis of LC3 was performed according to the standard method. Twenty micrograms of protein of each sample were loaded on 12.5% sodium dodecyl sulfate-polyacrylamide gel. After electrophoresis, the gel was transferred to polyvinylidene (PVDF) membrane and immunostained with anti-LC3 antibody. Data was analyzed by using LAS-1000 chemiluminescence imaging system (Fujifilm, Tokyo, Japan).

Quantitative real-time PCR. Total RNA was extracted from *Lmna*^{H222P/H222P} and wild-type MEF with TRIzol (Invitrogen) following manufacturer's protocol. Single-stranded cDNA was synthesized from RNA using SuperScript[™] III reverse transcriptase. Gene expression of LC3B was quantified by quantitative real-time PCR in Rotor-Gene[™] 6000 system (Corbett Life Science, NSW, Australia), using the following primers: LC3b-F; CCG AGA AGA CCT TCA AGC AG and LC3b-R; CCA TTC ACC AGG AGG AAG AA. All the results were normalized with respect to G3PDH expression.

Autophagy inhibition. MEF from *Lmna*^{H222P/H222P} mice and wild-type littermates were treated with 10 mM 3-MA (Sigma-Aldrich) and 200 nM wortmannin (Sigma-Aldrich), which are also known as phosphatidylinositol-3 kinase inhibitors and autophagy inhibitors, or negative control at 80% confluent state for 2 hours as previously described.⁴⁹ After the treatment, the amount of LC3 was measured by immunoblotting analysis. Immunocytochemistry of LC3 and a nuclear envelope protein (lamin C) was also performed to check the changes in nuclear abnormalities with autophagy inhibition. For the calculation of cell survival rate, the cells were stained by acetoxymethyl ester of calcein (Calcein-AM, Dojindo, MD) and propidium iodide (PI, Dojindo) for 15 min at 37°C according to the manufacturer's instruction. This staining method can differentiate green-colored viable and red-colored dead cells, respectively. Cell viability was determined as the ratio of the number of viable cells per total number of cells in four groups of untreated wild-type, treated wild-type, untreated *Lmna*^{H222P/H222P} and treated *Lmna*^{H222P/H222P} cells.

Statistical analyses. To get quantitative data, three to four replicates of measurement were done for each condition. All the data were presented as mean and standard deviation. Comparisons among groups were done by using student-t test and analysis of

variance (ANOVA) as appropriate. Statistical significance was considered when p value was less than 0.05.

Acknowledgements

We thank Drs. Colin L. Stewart (National Cancer Institute, MD, USA) and Dr. Noboru Mizushima (Tokyo Medical and Dental University, Tokyo) for providing mice of *Lmna*^{-/-} and GFP-LC3, respectively, and Dr. May Christine V. Malicdan (National Institute of Neuroscience, NINP) for reviewing the manuscript. This study was supported by the "Research on Psychiatric and Neurological Diseases and Mental Health" of "Health Labour Sciences Research Grant" and the "Research Grant (20B-12, 20B-13) for Nervous and Mental Disorders" from the Ministry of Health, Labor and Welfare; Human Frontier Science Program; Grant-in-Aid for Scientific Research from Japan Society for the Promotion of Science; Research on Publicly Essential Drugs and Medical Devices from the Japanese Health Sciences Foundation; and Program for Promotion of Fundamental Studies in Health Sciences of the National Institute of Biomedical Innovation (NIBIO).

Note

Supplementary materials can be found at: www.landesbioscience.com/supplement/ParkAUTO5-6-Sup.pdf

References

- Bonne G, Di Barletta MR, Varnous S, Becane HM, Hammouda EH, Medini L, et al. Mutations in the gene encoding lamin A/C cause autosomal dominant Emery-Dreifuss muscular dystrophy. *Nat Genet* 1999; 21:285-8.
- Raffaele Di Barletta M, Ricci E, Galluzzi G, Tomali R, Mora M, Morandi L, et al. Different mutations in the LMNA gene cause autosomal dominant and autosomal recessive Emery-Dreifuss muscular dystrophy. *Am J Hum Genet* 2000; 66:1407-12.
- Muchir A, Bonne G, van der Kooij AJ, van Meegen M, Bais E, Bolhuis PA, et al. Identification of mutations in the gene encoding lamins A/C in autosomal dominant limb girdle muscular dystrophy with atrioventricular conduction disturbances (LGMD1B). *Hum Mol Genet* 2000; 9:1453-9.
- Fatkin D, MacRae C, Sasaki T, Wolff MR, Porcu M, Frenneaux M, et al. Missense mutations in the rod domain of the lamin A/C gene as causes of dilated cardiomyopathy and conduction-system disease. *N Engl J Med* 1999; 341:1715-24.
- Becane HM, Bonne G, Varnous S, Muchir A, Ortega V, Hammouda EH, et al. High incidence of sudden death with conduction system and myocardial disease due to lamins A and C gene mutation. *Pacing Clin Electrophysiol* 2000; 23:1661-6.
- Cao H, Hegele RA. Nuclear lamin A/C R482Q mutation in canadian kindreds with Dunnigan-type familial partial lipodystrophy. *Hum Mol Genet* 2000; 9:109-12.
- De Sandre-Giovannoli A, Chaouch M, Kozlov S, Vallat JM, Tazir M, Kassouri N, et al. Homozygous defects in LMNA, encoding lamin A/C nuclear-envelope proteins, cause autosomal recessive axonal neuropathy in human (Charcot-Marie-Tooth disorder type 2) and mouse. *Am J Hum Genet* 2002; 70:726-36.
- De Sandre-Giovannoli A, Bernard R, Cau R, Navarro C, Amiel J, Boccaccio I, et al. Lamin A truncation in Hutchinson-Gilford progeria. *Science* 2003; 300:2055.
- Eriksson M, Brown WT, Gordon LB, Glynn MW, Singer J, Scott L, et al. Recurrent de novo point mutations in lamin A cause Hutchinson-Gilford progeria syndrome. *Nature* 2003; 423:293-8.
- Bione S, Maestri E, Rivella S, Mancini M, Regis S, Romeo G, Toniolo D. Identification of a novel X-linked gene responsible for Emery-Dreifuss muscular dystrophy. *Nat Genet* 1994; 8:323-7.
- Ura S, Hayashi YK, Goto K, Astejada MN, Murakami T, Nagato M, et al. Limb-girdle muscular dystrophy due to emerin gene mutations. *Arch Neurol* 2007; 64:1038-41.
- Karsz ML, Herron KJ, Olson TM. X-linked nonsyndromic sinus node dysfunction and atrial fibrillation caused by emerin mutation. *J Cardiovasc Electrophysiol* 2008; 19:510-5.
- Ben You R, Toutain A, Arimura T, Demay L, Massart C, Paccate C, et al. Multisubunit involvement in a family with LMNA and EMD mutations: Role of digenic mechanism? *Neurology* 2007; 68:1883-94.
- Broers JL, Peeters EA, Kuijpers HJ, Ender J, Bouten CV, Oomens CW, et al. Decreased mechanical stiffness in LMNA^{-/-} cells is caused by defective nucleo-cytoskeletal integrity: implications for the development of laminopathies. *Hum Mol Genet* 2004; 13:2567-80.

15. Lammerding J, Schulze PC, Takahashi T, Kozlov S, Sullivan T, Kamm RD, et al. Lamin A/C deficiency causes defective nuclear mechanics and mechanotransduction. *J Clin Invest* 2004; 113:370-8.
16. Sakaki M, Koike H, Takahashi N, Sasagawa N, Tamioka S, Arahata K, Ishiura S. Interaction between emerin and nuclear lamins. *J Biochem* 2001; 129:321-7.
17. Mislav JM, Holaska JM, Kim MS, Lee KK, Segura-Totten M, Wilson KL, McNally EM. Nesprin-1alpha self-associates and binds directly to emerin and lamin A in vitro. *FEBS Lett* 2002; 525:135-40.
18. Bengtsson L, Wilson KL. Multiple and surprising new functions for emerin, a nuclear membrane protein. *Curr Opin Cell Biol* 2004; 16:73-9.
19. Zhang Q, Ragnauth CD, Skepper JN, Worth NR, Warren DT, Roberts RG, et al. Nesprin-2 is a multi-isomeric protein that binds lamin and emerin at the nuclear envelope and forms a subcellular network in skeletal muscle. *J Cell Sci* 2005; 118:673-87.
20. Sabatelli P, Lattanzi G, Ognibene A, Columbaro M, Capanni C, Merlini L, et al. Nuclear alterations in autosomal-dominant Emery-Dreifuss muscular dystrophy. *Muscle Nerve* 2001; 24:826-9.
21. Park YE, Hayashi YK, Goto K, Nonaka I, Noguchi S, Nishino I. Nuclear Changes in Skeletal Muscles Extend to Satellite Cells in AD-EDMD/LGMD1B. *Neuromuscul Disord* 2008; In Press.
22. Fidzianska A, Toniolo D, Hausmanowa-Petrusewicz I. Ultrastructural abnormality of sarcolemmal nuclei in Emery-Dreifuss muscular dystrophy (EDMD). *J Neurol Sci* 1998; 159:88-93.
23. Fidzianska A, Hausmanowa-Petrusewicz J. Architectural abnormalities in muscle nuclei. Ultrastructural differences between X-linked and autosomal dominant forms of EDMD. *J Neurol Sci* 2003; 210:47-51.
24. Fidzianska A, Bilinska ZT, Tesson F, Wagner T, Walski M, Grzybowski J, et al. Obliteration of cardiomyocyte nuclear architecture in a patient with LMNA gene mutation. *J Neurol Sci* 2008; 271:91-6.
25. Ozawa R, Hayashi YK, Ogawa M, Kurokawa R, Matsumoto H, Noguchi S, et al. Emerin-lacking mice show minimal motor and cardiac dysfunctions with nuclear-associated vacuoles. *Am J Pathol* 2006; 168:907-17.
26. Harding TM, Morano KA, Scott SV, Klionsky DJ. Isolation and characterization of yeast mutants in the cytoplasm to vacuole protein targeting pathway. *J Cell Biol* 1995; 131:591-602.
27. Klionsky DJ, Clegg JM, Dunn WA Jr, Emr SD, Sakai Y, Sandoval IV, et al. A unified nomenclature for yeast autophagy-related genes. *Dev Cell* 2003; 5:539-45.
28. Taniida I, Ueno T, Kominami E. LC3 conjugation system in mammalian autophagy. *Int J Biochem Cell Biol* 2004; 36:2503-18.
29. Dunn WA Jr, Clegg JM, Kiel JA, van der Klei IJ, Oku M, Sakai Y, et al. Pexophagy: the selective autophagy of peroxisomes. *Autophagy* 2005; 1:75-83.
30. Kim I, Rodriguez-Enriquez S, Lemasters JJ. Selective degradation of mitochondria by mitophagy. *Arch Biochem Biophys* 2007; 462:245-53.
31. Bernales S, Schuck S, Walter P. ER-phagy: selective autophagy of the endoplasmic reticulum. *Autophagy* 2007; 3:285-7.
32. Muchir A, van Engelen BG, Lammens M, Mislav JM, McNally E, Schwartz K, Bonnie G. Nuclear envelope alterations in fibroblasts from LGMD1B patients carrying nonsense Y259X heterozygous or homozygous mutation in lamin A/C gene. *Exp Cell Res* 2003; 291:352-62.
33. Muchir A, Medioni J, Laluc M, Massart C, Arimura T, van der Kooij AJ, et al. Nuclear envelope alterations in fibroblasts from patients with muscular dystrophy, cardiomyopathy and partial lipodystrophy carrying lamin A/C gene mutations. *Muscle Nerve* 2004; 30:444-50.
34. Kabeya Y, Mizushima N, Ueno T, Yamamoto A, Kirisako T, Noda T, et al. LC3, a mammalian homologue of yeast Apg8p, is localized in autophagosomal membranes after processing. *EMBO J* 2000; 19:5720-8.
35. Mizushima N, Yamamoto A, Matsui M, Yoshimori T, Ohsumi Y. In vivo analysis of autophagy in response to nutrient starvation using transgenic mice expressing a fluorescent autophagosomal marker. *Mol Biol Cell* 2004; 15:1101-11.
36. Xie Z, Klionsky DJ. Autophagosome formation: core machinery and adaptations. *Nat Cell Biol* 2007; 9:1102-9.
37. Young AR, Chan EY, Hu XW, Kochl R, Crawshaw SG, High S, et al. Starvation and ULK1-dependent cycling of mammalian Atg9 between the TGN and endosomes. *J Cell Sci* 2006; 119:3888-900.
38. Gutierrez MC, Munafò DB, Beton W, Colombo MI. Rab7 is required for the normal progression of the autophagic pathway in mammalian cells. *J Cell Sci* 2004; 117:2687-97.
39. Fillingham J, Keogh MC, Krogan NJ. GammaH2AX and its role in DNA double-strand break repair. *Biochem Cell Biol* 2006; 84:568-77.
40. Taniida I, Minematsu-Ikeguchi N, Ueno T, Kominami E. Lysosomal turnover, but not a cellular level, of endogenous LC3 is a marker for autophagy. *Autophagy* 2005; 1:84-91.
41. Nakagawa I, Amano A, Mizushima N, Yamamoto A, Yamaguchi H, Kamimoto T, et al. Autophagy defends cells against invading group A *Streptococcus*. *Science* 2004; 306:1037-40.
42. Kvam E, Goldfarb DS. Nucleus-vacuole junctions and piecemeal microautophagy of the nucleus in *S. cerevisiae*. *Autophagy* 2007; 3:85-92.
43. Kvam E, Goldfarb DS. Nucleus-vacuole junctions in yeast: anatomy of a membrane contact site. *Biochem Soc Trans* 2006; 34:340-2.
44. Krick R, Muehe Y, Prick T, Breuer S, Schlotterhose P, Eskelinen EL, et al. Piecemeal microautophagy of the nucleus requires the core macroautophagy genes. *Mol Biol Cell* 2008; 19:4492-505.
45. Marino G, Ugalde AP, Salvador-Montoliu N, Varela I, Quiros PM, Cadinanos J, et al. Premature aging in mice activates a systemic metabolic response involving autophagy induction. *Hum Mol Genet* 2008; 17:2196-211.
46. Pentdas AM, Zhou Z, Cadinanos J, Freije JM, Wang J, Hultenby K, et al. Defective prelamin A processing and muscular and adipocyte alterations in Zmpste24 metalloproteinase-deficient mice. *Nat Genet* 2002; 31:94-9.
47. Arimura T, Helbling-Ledet A, Massart C, Varnous S, Niel F, Lacene E, et al. Mouse model carrying H222P-Lmna mutation develops muscular dystrophy and dilated cardiomyopathy similar to human striated muscle laminopathies. *Hum Mol Genet* 2005; 14:155-69.
48. Sullivan T, Escalante-Alcalde D, Bhatt H, Anvet M, Bhat N, Nagashima K, et al. Loss of A-type lamin expression compromises nuclear envelope integrity leading to muscular dystrophy. *J Cell Biol* 1999; 147:913-20.
49. Carra S, Seguin SJ, Lambert H, Landry J. HspB8 chaperone activity toward poly(IQ)-containing proteins depends on its association with Bag3, a stimulator of macroautophagy. *J Biol Chem* 2008; 283:1437-44.



Human *PTRF* mutations cause secondary deficiency of caveolins resulting in muscular dystrophy with generalized lipodystrophy

Yukiko K. Hayashi,¹ Chie Matsuda,² Megumu Ogawa,¹ Kanako Goto,¹ Kayo Tominaga,¹ Satomi Mitsuhashi,¹ Young-Eun Park,¹ Ikuya Nonaka,¹ Naomi Hino-Fukuyo,³ Kazuhiro Haginoya,^{3,4} Hisashi Sugano,⁵ and Ichizo Nishino¹

¹Department of Neuromuscular Research, National Institute of Neuroscience, National Center of Neurology and Psychiatry, Kodaira, Tokyo, Japan.

²Neuroscience Research Institute, National Institute of Advanced Industrial Science and Technology, Tsukuba, Ibaraki, Japan. ³Department of Pediatrics, Tohoku University School of Medicine, Sendai, Miyagi, Japan. ⁴Department of Pediatric Neurology, Takuto Rehabilitation Center for Children, Sendai, Miyagi, Japan. ⁵Department of Metabolic and Endocrine Medicine, Kochi Health Science Center, Kochi, Kochi, Japan.

Caveolae are invaginations of the plasma membrane involved in many cellular processes, including clathrin-independent endocytosis, cholesterol transport, and signal transduction. They are characterized by the presence of caveolin proteins. Mutations that cause deficiency in caveolin-3, which is expressed exclusively in skeletal and cardiac muscle, have been linked to muscular dystrophy. Polymerase I and transcript release factor (*PTRF*; also known as cavin) is a caveolar-associated protein suggested to play an essential role in the formation of caveolae and the stabilization of caveolins. Here, we identified *PTRF* mutations in 5 nonconsanguineous patients who presented with both generalized lipodystrophy and muscular dystrophy. Muscle hypertrophy, muscle mounding, mild metabolic complications, and elevated serum creatine kinase levels were observed in these patients. Skeletal muscle biopsies revealed chronic dystrophic changes, deficiency and mislocalization of all 3 caveolin family members, and reduction of caveolae structure. We generated expression constructs recapitulating the human mutations; upon overexpression in myoblasts, these mutations resulted in *PTRF* mislocalization and disrupted physical interaction with caveolins. Our data confirm that *PTRF* is essential for formation of caveolae and proper localization of caveolins in human cells and suggest that clinical features observed in the patients with *PTRF* mutations are associated with a secondary deficiency of caveolins.

Introduction

Caveolae are specific invaginations of the plasma membrane characterized by the presence of the protein caveolin. To date, 3 caveolin family members have been identified. Caveolin-1 and -2 are coexpressed in many cell types, such as endothelial cells, smooth muscle cells, fibroblasts, and adipocytes, and form a hetero-oligomeric complex (1). In contrast, caveolin-3 is expressed exclusively in skeletal and cardiac muscles (2). Caveolae are involved in several important cellular processes, including clathrin-independent endocytosis, regulation and transport of cellular cholesterol, and signal transduction (3, 4).

Polymerase I and transcript release factor (*PTRF*; also known as cavin) is a highly abundant caveolae component and is suggested to have an essential role in caveolar formation. In both mammalian cells and zebrafish, knockdown of *PTRF* leads to a reduction in caveolae density (5). Mice lacking *PTRF* do not have morphologically detectable caveolae, in addition to a markedly diminished protein expression of all 3 caveolin isoforms (6). Interestingly, *PTRF*-knockout mice mimic lipodystrophy in humans, demonstrating considerably reduced adipose tissue mass, high circulating triglyceride levels, glucose intolerance, and hyperinsulinemia (6).

Here we report that mutations in *PTRF* (GenBank accession no. 284119) caused a disorder presenting as generalized lipodystrophy and muscular dystrophy. We demonstrate that this condition was associated with deficiency and mislocalization of all 3 caveolin family members and reduction of caveolae structure.

Results

Identification of *PTRF* mutations. Deficiency of caveolin-3 as a result of *CAV3* gene mutations is known to cause muscular dystrophy (7). We found 5 nonconsanguineous Japanese patients whose muscle showed caveolin-3 deficiency but without *CAV3* mutation among 2,745 muscular dystrophy specimens kept in the muscle repository of the National Center of Neurology and Psychiatry. Importantly, all 5 patients also had congenital generalized lipodystrophy (CGL; also known as Berardinelli-Seip syndrome). From the findings observed in lacking cells and animal models lacking *PTRF* (5, 6), we screened for *PTRF* mutations.

We identified 2 different frameshift mutations in all 5 patients examined: patients 1–4 (P1–P4) had the same homozygous c.696_697insC (p.K233fs) mutation in exon 2, and P5 harbored a compound heterozygous mutation of the same c.696_697insC and c.525delG (p.E176fs) in exon 2 (Figure 1A). The c.525delG mutation changes the last 275 amino acids to an unrelated 98-amino acid sequence, whereas c.696_697insC substitutes the last 158 amino acids with an unrelated 191-amino acid sequence (Figure 1B). Both mutations were not identified in the chromosomes of 200 Japanese control subjects.

In order to determine whether the common c.696_697insC mutation has the same haplotype, we examined 6 sets of single nucleotide polymorphisms (SNPs) within *PTRF*: rs2062213, rs8070945, rs963988, rs963987, rs963986, and rs9252. All 5 patients had the same haplotype for all 6 SNPs, which occurred homozygously (Table 1). During mutation screening, we found a novel 9-bp insertion polymorphism in the 3' noncoding region

Conflict of interest: The authors have declared that no conflict of interest exists.

Citation for this article: *J Clin Invest* 119:2623–2633 (2009) doi:10.1172/JCI38660.

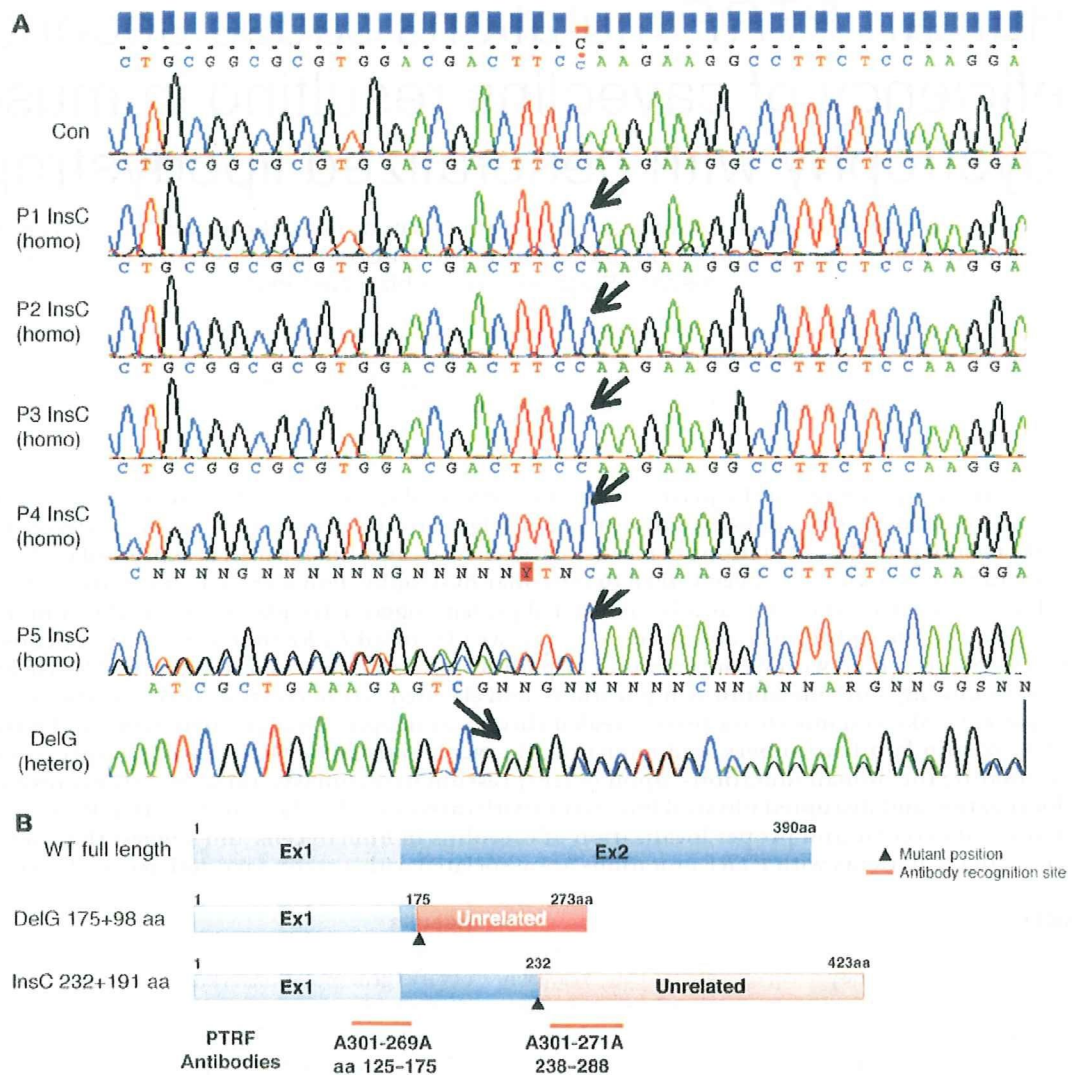


Figure 1 Mutations in *PTRF*. (A) All 5 patients had a homozygous or compound heterozygous mutation in *PTRF* (shown by arrows). P1–P4 had the same homozygous insertion mutation of c.696_697insC (InsC) in exon 2, whereas P5 had a compound heterozygous mutation of the same c.696_697insC insertion mutation and a deletion mutation of c.525delG (DelG) in exon 2. (B) Schema of the position of mutations in *PTRF*, putative proteins produced by mutations, and antibody recognition sites. The c.525delG mutant changes the last 275 amino acids to an unrelated 98–amino acid sequence, while the c.696_697insC mutant substitutes the last 158 amino acids with an unrelated 191–amino acid sequence.

of *PTRF* (c.1235_1236insTCTCGGCTC). This 9-bp insertion was found heterozygously in 26% and homozygously in 2% of Japanese control individuals. In P1–P5, none had this 9-bp insertion. We also examined 2 microsatellite markers (STS-W93348 and D17S1185) close to *PTRF* and found heterozygosity in the patients (Table 1). From these results, a founder effect may not be likely, although we could not completely rule out the possibility.

Mutation screening of the other genes associated with lipodystrophy and muscular dystrophy. From the clinical and pathological findings, we performed mutation screening for the genes associated with muscular dystrophy and lipodystrophy, including *CAV3*, *LMNA*, *AGPAT2*, *BSC12*, *CAVI*, *PPARG*, *AKT2*, and *ZMPSTE24*. We found a heterozygous nucleotide change of c.1138G>A (p.D380N) in *BSC12* in P1. This substitution was also identified heterozygously

in 16% of Japanese control individuals, and we believe this to be a novel nonsynonymous SNP. For all the other genes examined, no other mutation was identified in P1–P5.

Clinical features of the patients with PTRF mutations. Clinical information for P1–P5 is summarized in Table 2. Common to all patients was the presence of muscular dystrophy and generalized lipodystrophy. However, despite having the same mutation, the patients' additional symptoms were variable. Generalized loss of subcutaneous adipose tissue in several areas, including the face, was noticed in infancy or early childhood. Hepatosplenomegaly, acromegaly features, and umbilical prominence were often observed in the patients. No patient showed intellectual deficit or acanthosis nigricans. Patients presented with mild muscle weakness, but with hypertrophy of muscles (Figure 2A). Electrically silent percussion-induced

Table 1
Haplotype analysis

	P1	P2	P3	P4	P5	Control ^A
Intron 1, rs2062213	C/C	C/C	C/C	C/C	C/C	C/C (53%)
Intron 1, rs8070945	C/C	C/C	C/C	C/C	C/C	C/C (78%)
Intron 1, rs963988	G/G	G/G	G/G	G/G	G/G	G/G (33%)
Intron 1, rs963987	G/G	G/G	G/G	G/G	G/G	G/G (31%)
Intron 1, rs963986	G/G	G/G	G/G	G/G	G/G	G/G (34%)
Exon 2, 9-bp insertion ^B	no/no	no/no	no/no	no/no	no/no	no/no (72%)
Exon 2, rs9252 ^B	C/C	C/C	C/C	C/C	C/C	C/C (78%)
STS-W93348 (bp)	251/253	251/253	251/253	251/253	251/253	251/253/264
D17S1185 (bp)	219/219	170/219	170/219	170/170	170/203	170/203/215/219/225/237

^APercentages denote the frequency of the haplotype in the HapMap JPT population. ^BExon 2 is 3' noncoding.

muscle mounding was characteristic. Cardiac arrhythmia, transient immunodeficiency, recurrent pneumonia, constipation, and chaliasia were variably seen. Available laboratory data in the patients are summarized in Table 3. Metabolic complication was mild, and none of our patients showed marked elevation of fasting glucose levels. The result of oral glucose tolerance tests revealed moderate fasting hyperinsulinemia in P1 and P2 associated with glucose intolerance in P2, but normal levels in P4 (Table 4). High triglyceremia was seen in P4 and P5. Serum creatine kinase (CK) levels were moderately elevated in all patients. Abdominal CT images of P4 revealed marked loss of subcutaneous and intra-abdominal fat (Figure 2, B and C). In addition, his body fat ratio, as determined by whole body dual energy X-ray absorptiometry, was 7.1% (Supplemental Table 1; supplemental material available online with this article; doi:10.1172/JCI38660DS1), while head fat was relatively preserved.

Clinical features of the heterozygous parents. There was no family history of muscular dystrophy or lipodystrophy in P1-P5. Genetic

analysis revealed a heterozygous c.696_698insC mutation in both parents of P4. Clinically, both father and mother had hypertension requiring medication, whereas P4 was normotensive. Mild lipid metabolism abnormality and borderline glucose intolerance was also seen (Supplemental Table 2). DNA samples from the other parents were not available.

Loss of PTRF with deficiency or mislocalization of caveolins in skeletal muscle. Biopsied skeletal muscles from P1-P5 showed consistent findings, with chronic dystrophic changes including marked variation in muscle fiber size, increased number of fibers containing internalized nuclei, a few necrotic and regenerating fibers, and increased interstitial fibrosis (Figure 2D and Supplemental Figure 1). Intramuscular lipid droplets, as visualized by oil red O staining, were not increased (Figure 2D).

Immunohistochemistry demonstrated that the PTRF antibodies A301-269A and A301-271A (which recognize the N- and C-terminal regions of the protein, respectively; Figure 1B) showed sarcolemmal membrane staining of muscle fibers, with stronger immunoreaction at intramuscular blood vessels in control muscles (Figure 3A). Caveolin-3 was clearly observed at sarcolemma, whereas caveolin-1 and -2 were present only in blood vessels. In contrast, muscles from P1-P5 showed barely detectable immunoreaction to both PTRF antibodies (Figure 3A). Caveolin-3 immunoreactivity was greatly reduced in the sarcolemma, but cytoplasmic staining was remarkably increased. This caveolin-3 staining pattern was similar to that seen in the patients with muscular dystrophy

Table 2
Clinical summary

	P1	P2	P3	P4	P5
Age/sex	8-yr-old female	14-yr-old female	10-yr-old male	27-yr-old male	24-yr-old male
Height, body weight	124 cm, 21.3 kg	149 cm, 40.5 kg	NA	164 cm, 49.0 kg	152 cm, 40 kg
Lipodystrophy	Generalized	Generalized	Generalized	Generalized	Generalized
Mental retardation	No	No	No	No	No
Acanthosis nigricans	No	No	No	No	No
Liver/spleen	Hepatosplenomegaly	Fatty liver	NA	Hepatosplenomegaly	No
Endocrine abnormalities	Reduced growth hormone secretion	NA	NA	Accelerated bone age, acromegaloid features, no androgynism	Acromegaloid features, no androgynism
Muscle weakness	Distal dominant	No	No	Generalized	Distal dominant
Muscle mounding	Positive	NA	NA	Positive	Positive
Other muscle symptoms	Muscle hypertrophy	Myalgia, muscle stiffness	NA	Muscle hypertrophy	Muscle hypertrophy
Cardiac symptoms	Arrhythmia	No	No	Atrial fibrillation	No
Skeletal abnormalities	Lordosis, Contractures (ankles, shoulders, fingers)	No	No	Scoliosis, contractures (ankles)	Scoliosis
Other symptoms	Constipation	Transient IgA deficiency, recurrent pneumonia	Nephrosis	Umbilical prominence, renal stones	Recurrent pneumonia, chaliasia constipation

NA, not available.

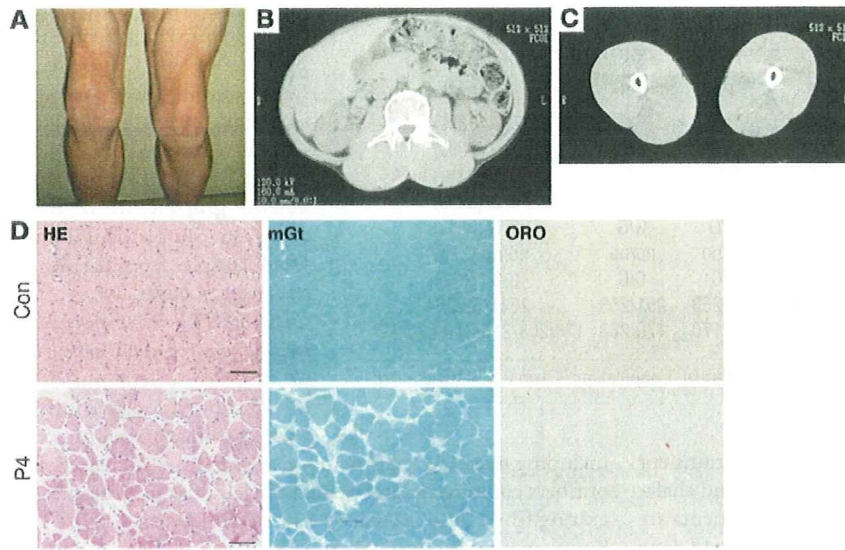


Figure 2
Muscle hypertrophy and dystrophic changes. (A) Prominent musculature feature of legs in P5. (B and C) CT images from P4 showed hypertrophy of paravertebral and thigh muscles with minimal subcutaneous and intra-abdominal fat tissue. (D) H&E stain of biopsied skeletal muscle from P4 showed dystrophic changes, including marked variation in fiber size, enlarged fibers with internalized nuclei, endomysial fibrosis, and few necrotic and regenerating fibers. Intramuscular lipid droplets were not increased compared with control. mGt, modified Gomori trichrome; ORO, oil red O. Scale bars: 50 μ m.

caused by *CAV3* mutations (data not shown). Similarly, dysferlin was decreased in the sarcolemma and mislocalized into the cytoplasm (data not shown), and the same pattern is also seen in muscles of individuals with *CAV3* mutations (8). Immunoreactivity to caveolin-1 and caveolin-2 in blood vessels was barely detectable in P1-P5 (Figure 3A). Other antibodies related to muscular dystrophy, including dystrophin, sarcoglycans, dystroglycans, emerin, merosin, and collagen VI, showed normal immunostaining patterns (data not shown).

Immunoblotting showed detection of PTRF as an approximately 50-kDa band in control muscles and 3T3 cells, which were used as a positive control. No band was detected in the muscle of P1-P5 (Figure 3B). Caveolin-3 was detected in all samples examined, but relative protein amount, determined using densitometry and normalized by myosin heavy chain (MHC), decreased in P1-P5 compared with control subjects (Figure 3C). The band for caveolin-2 was observed in control muscles and 3T3 cells, but was barely detectable in the muscles of P1-P5 (Figure 3B).

In order to determine mRNA expression of PTRF, RT-PCR was performed using total RNA extracted from biopsied skeletal muscles. Using primers designed to amplify whole coding region of mRNA, PTRF was amplified as a single transcript in control muscles. In contrast, no PCR product was amplified in P1-P5 (Figure 4A). To compare mRNA levels for caveolins, we performed quantitative RT-PCR and normalized results to GAPDH expression. The mRNA amounts of all 3 caveolin families in the patients' muscles were variable, but not markedly decreased, compared with control muscles (Figure 4, B and C). Preserved mRNA levels, but decreased protein amounts of caveolins, suggested destabilization of caveolin proteins when PTRF is lacking, as previously reported (9).

Loss of PTRF causes reduced caveolae formation in human muscles. Greatly reduced caveolae formation was previously reported in PTRF knockdown

mammalian cells, zebrafish, and knockout mice (5, 9). Decreased caveolae number was also reported in skeletal muscle from limb girdle muscular dystrophy type 1C (LGMD1C) patients with *CAV3* mutations (10). We therefore examined muscle caveolae in P2 and P3 using electron microscopy. Plasma membrane of muscle fibers from both patients was nearly flat, and caveolae density was notably reduced, compared with control muscle (Figure 5). Caveolae formation in the intramuscular vascular smooth muscle cells was also remarkably reduced (data not shown).

Altered localization of mutant PTRF and reduced interaction with caveolins in transfected cells. In order to determine the intracellular localization of mutant PTRF, FLAG-tagged WT or 2 mutants (c.525delG and c.696_697insC) and T7-tagged caveolin-3 or -1 were cotransfected in C2C12 myoblasts and COS-7 cells. In C2C12 cells, WT PTRF was detected at the cell membrane and colocalized with caveolin-3 (Figure 6A). Interestingly, c.525delG was detected as intranuclear aggregations and was not observed at the cell membrane (Figure 6, A and B). Caveolin-3 was present only in cytoplasm, and did not merge with PTRF (Figure 6A). The c.696_697insC mutant was observed as microtubular filament network in cytoplasm and colocalized with β -tubulin (Figure 6B). This finding is consistent with the localization of the truncated PTRF₁₋₃₂₂, as described previously (9). Similar mislocalization and/or aggregation of transfected mutant PTRF was observed in COS-7 cells (data not shown).

Table 3
Laboratory data

Measurement	Reference range	P1	P2	P3	P4	P5
CK (IU/l)	56-244	1,374	542-2,253	2,000	554-1,545	645-2,630
Fasting glucose (mg/dl)	70-109	75	99	NA	93-116	102
HbA1c (%)	4.3-5.8	NA	NA	NA	5.0-5.4	NA
Total cholesterol (mg/dl)	130-220	164	NA	NA	185-267	218
Triglyceride (mg/dl)	50-150	93	NA	NA	143-450	359
LDL-C (mg/dl)	70-139	NA	NA	NA	188	NA
Leptin (ng/ml)	0.9-13.0	NA	NA	NA	0.6	NA
Adiponectin (μ g/ml)	None	NA	NA	NA	1.05	NA

NA, not available

Table 4
Oral glucose tolerance test of P1, P2, and P4

	Pre	30 min	60 min	120 min
P1				
Glucose (mg/dl)	75	98	69	62
IRI (μ U/ml)	22.8	141.6	64.7	23.8
P2				
Glucose (mg/dl)	99	127	160	172
IRI (μ U/ml)	20	53	65	80
P4				
Glucose (mg/dl)	93	124	140	70
CPR (ng/ml) ^A	2.8	5.9	8.3	5.5
IRI (μ U/ml)	1.0	22.3	32.9	6.2

IRI, immunoreactive insulin; CPR, C-peptide immunoreactivity. ^AReference range, 0.7–2.2 ng/ml.

We performed immunoprecipitation assay in order to examine the binding ability of PTRF and caveolins. WT PTRF was coimmunoprecipitated by anti-T7 antibody, and vice versa (Figure 6, C and D). The c.525delG mutant showed smaller molecular weight (estimated 30 kDa; Figure 1B), and no immunoprecipitated protein was detected by FLAG and T7 antibodies. The c.696_697insC mutant showed slightly larger molecular weight, and coimmunoprecipitated proteins were greatly reduced (Figure 6, C and D). These results suggest that mutant PTRFs cannot localize properly and lose their binding ability to caveolins even if they are produced.

Activation of myostatin and Akt signaling pathways in PTRF-deficient skeletal muscles. Caveolin-3 is suggested to have an important role for suppression of myostatin-mediated signaling in skeletal muscle (11). In order to determine the functions of mislocalized caveolin-3 in PTRF mutated cells, we performed quantitative RT-PCR for myostatin and immunoblotting analysis to examine phosphorylation status of Mad homolog 2/3 (p-Smad2/3), an intracellular effector of myostatin in skeletal muscles. In P1–P5, increased amounts of p-Smad2/3^{S423/425} were observed in skeletal muscles, while myostatin mRNA levels were variable (Figure 7, A–C). Positive immunoreaction to p-Smad2/3 was detected in few myonuclei from muscle of patients with PTRF or CAV3 mutations, but not in those from muscle of control subjects (data not shown). These results suggest that myostatin signaling is also activated in P1–P5.

Despite the activation of myostatin, a negative regulator of muscle growth, the patients showed hypertrophy of muscles. Since Akt (also known as protein kinase B) is known as the key molecule to regulate muscle mass (12), we examined p-Akt^{T308} and p-Akt^{S473} by immunoblotting analysis. p-Akt was elevated in the muscle of P1–P5 compared with controls, except for p-Akt^{S473} in P2 (Figure 7, D–F). This result suggests that Akt pathway is activated, probably through an as-yet-unidentified mechanism, and could contribute to the muscle hypertrophy observed in P1–P5.

Neuronal NOS activity is variable and mildly increased in PTRF-deficient skeletal muscles. Caveolin-3 is known to interact with and negatively regulate the catalytic activity of neuronal NOS (nNOS) in skeletal muscle (13); this notion is supported by the finding of increased nNOS activity in muscle of transgenic mice expressing mutant caveolin-3 (14). We thus examined nNOS expression and its activity in muscles from patients with mutations in PTRF or CAV3 compared with those from age-matched controls. The immunoreactivity of nNOS was seen in sarcolemma and cytoplasm of

each muscle fiber with variable intensity, but no obvious difference was seen between patients and controls (Figure 3A). Immunoblotting analysis also revealed comparable amounts of nNOS (Figure 3, B and D). In order to examine nNOS activity of each muscle fiber, we performed NADPH diaphorase (NDP) activity assay. The intensity of NDP staining appeared variable among muscle fibers and was slightly increased in patients with mutations in PTRF or CAV3 compared with age-matched controls (Figure 8).

Discussion

Lipodystrophy is a heterogeneous group of disorders characterized by loss of adipose tissue from the body. The degree of fat loss varies from small areas to near-complete absence of adipose tissue. The extent of fat loss usually determines clinical severity and metabolic complications, such as insulin resistance and high levels of serum triglycerides.

Several genes responsible for inherited lipodystrophy have been identified. CGL is an autosomal-recessive disorder, with most patients presenting soon after birth with severe insulin resistance and elevated serum triglycerides. CGL1 is caused by mutations in *AGPAT2* on chromosome 9q34, which encodes 1-acylglycerol-3-phosphate-O-acyltransferase 2, an enzyme involved in the biosynthesis of triacylglycerol and glycerophospholipids (15). CGL2 is caused by mutations in *BSCL2* on chromosome 11q13, which encodes a functionally unknown protein named seipin (16). Recently, mutations in *CAV1* on chromosome 7q31 have been reported to cause generalized (i.e., CGL3) and partial lipodystrophy (17, 18).

Several causative genes for autosomal-dominant familial partial lipodystrophy are known: *LMNA* on chromosome 1q21 (19), *ZMPSTE24* on chromosome 1p34 (20), *AKT2* on chromosome 19q13 (21), *PPARG* on chromosome 3p25 (22), and *LMNB2* on chromosome 19q1 (23). Nevertheless, many patients clinically diagnosed with lipodystrophy carry no mutation in the known genes, suggesting the presence of other causative genes.

Here we conclude that PTRF mutations can cause CGL. In our series, patients showed generalized loss of adipose tissue from infancy or early childhood. Because PTRF is reported to colocalize with hormone-sensitive lipase and translocate to the nucleus in the presence of insulin in adipocytes (24), it could be surmised that PTRF plays an important role in lipid metabolism and insulin-regulated gene expression. Interestingly, metabolic complications were milder in patients with PTRF mutations than in patients with CGL1 and CGL2, and these were observed only in the elder patients. Although we could not examine the status of caveolae and caveolins in adipose tissues, the secondary deficiency of caveolins might have an important role in the process of lipodystrophy, since *CAV1* mutation can cause lipodystrophy in both humans and mice (17, 18, 25). Notably, the heterozygous parents had mild metabolic disorders, but a robust conclusion could not be reached, as a limited number of the heterozygous carriers of the PTRF mutation were available to us. Further investigation is needed to determine the effect of haploinsufficiency of PTRF.

Skeletal muscle symptoms with serum CK elevation represent another common symptom in patients with PTRF mutations. The clinical and pathological findings are very similar to those observed in patients with CAV3 mutation (7, 26–28), although P1–P5 had no CAV3 mutations. The secondary loss of caveolin-3 in the sarcolemma may contribute to the muscle phenotype. Moreover, serum CK elevation may be a good laboratory marker for diagnosis of lipodystrophy patients with PTRF mutations.

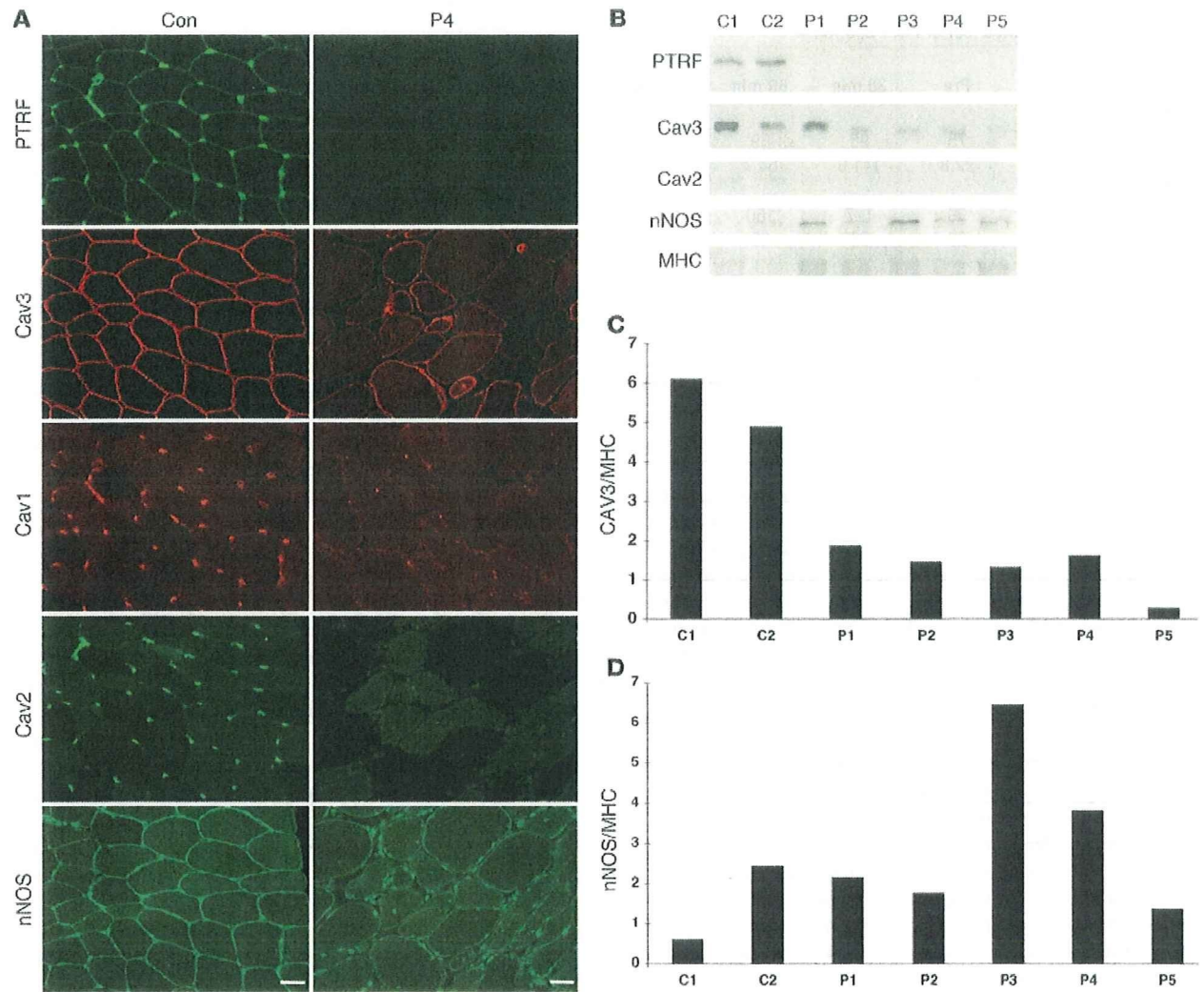


Figure 3

Loss of PTRF is associated with deficiency and mislocalization of caveolins in muscle. (A) In control muscle, PTRF was clearly seen in sarcolemma as strongly staining blood vessels. Caveolin-3 (Cav3) was clearly visible at sarcolemma, and caveolin-1 and -2 stained intramuscular blood vessels. The muscle of P4 was negative for PTRF. Membrane staining of caveolin-3 was reduced with increased cytoplasmic staining, and caveolin-1 and -2 were barely detectable. Immunoreactivity of nNOS varied between muscle fibers, but was not markedly different between control and patient muscle. Scale bar: 50 μ m. (B) Immunoblotting analysis of skeletal muscles. 3T3 cells were used as a positive control. PTRF and caveolin-2 were seen only in the muscles of 2 control subjects and in 3T3 cells, and were barely detectable in the muscles of P1–P5. The bands for caveolin-3 and nNOS were variably seen. (C and D) Quantification of immunoreactive bands was performed by densitometric analysis and normalized with MHC. In P1–P5, relative amounts of caveolin-3 decreased compared with control subjects (C), whereas nNOS amounts varied (D).

Caveolin-3 was previously reported to have an important role in inhibition of myostatin signaling by suppressing activation of its type I receptor. In mutant *Cav3* transgenic mice, loss of caveolin-3 causes muscular atrophy with increased p-Smad2, and this muscle atrophy can be rescued by myostatin inhibition (11). Consistent with the secondary reduction of caveolin-3, skeletal muscles from P1–P5 showed increased amounts of p-Smad2/3. Unexpectedly, however, muscle hypertrophy was seen in these patients.

The Akt pathway, when activated, is known to promote protein synthesis, stimulate muscle hypertrophy, and inhibit atrophy-related gene expression by phosphorylating FoxO transcription factors (12). This pathway is also known to play a pivotal role

in the regulation of glucose transport and glycogen synthesis in skeletal muscle cells. Akt is activated by insulin, various growth factors, nutrients, and exercise, whereas it is negatively regulated by myostatin and cytokines. Akt is phosphorylated at T308 by phosphoinositide-dependent kinase and at S473 by mammalian target of rapamycin in association with rictor. The increase in phosphorylated Akt in the muscle of P1–P5 may explain, at least in part, the muscle hypertrophy observed. Akt pathway activation might be associated with the metabolic complications observed in P1–P5. However, the upregulation of myostatin observed is contradictory to the established knowledge on muscle hypertrophy. This would be worthwhile to investigate in future studies, in order to

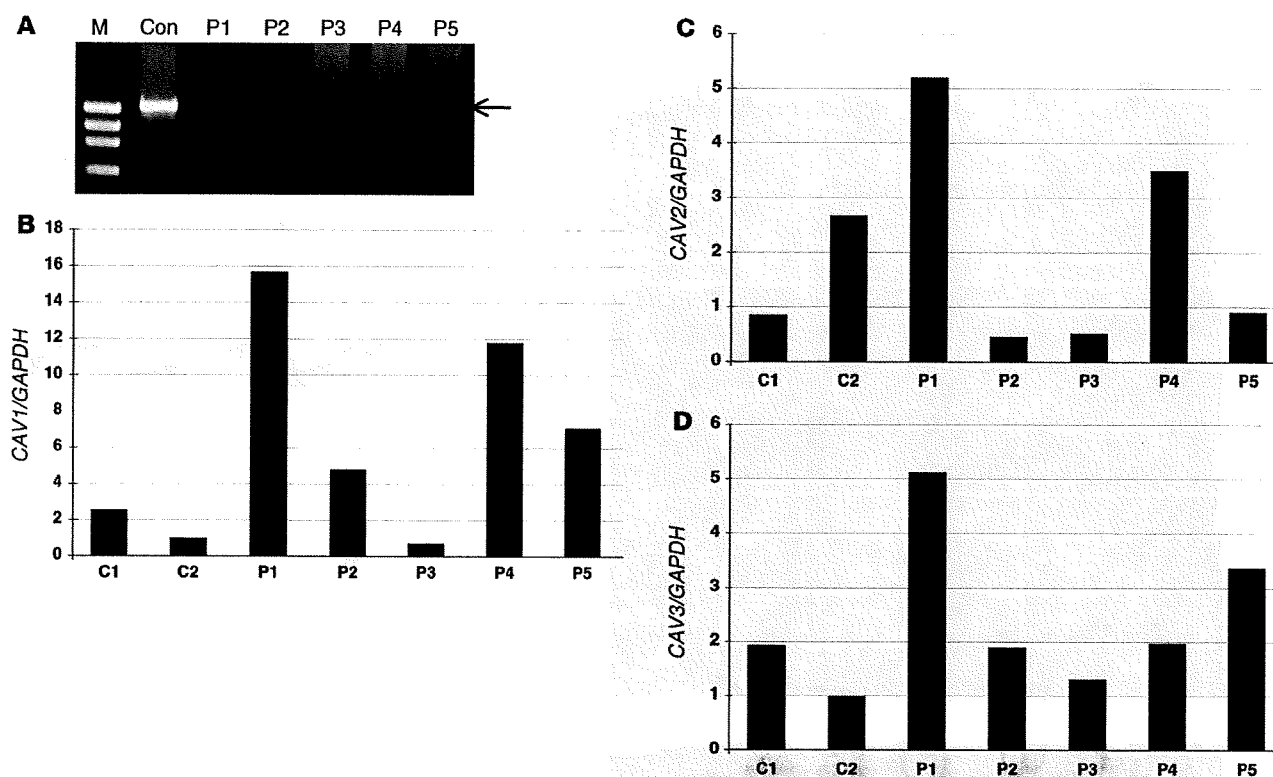


Figure 4 mRNA expression of PTRF in skeletal muscle, and quantitative RT-PCR of mRNAs for caveolins. (A) RT-PCR analysis revealed a single band for *PTRF* mRNA (arrow) in a control subject, but no detectable product was seen in P1–P5. M, marker. (B–D) By quantitative RT-PCR, mRNA for *CAV1*, *CAV2*, and *CAV3* normalized with *GAPDH* expression was not decreased in P1–P5.

elucidate the role of *PTRF* deficiency in muscle hypertrophy and related signaling pathway.

In addition to lipodystrophy and muscular dystrophy, P1–P5 had various other symptoms, whose association to *PTRF* mutation might be difficult to ascertain at this time. For example, 2 of 5 patients had arrhythmia. Although we could not examine the expression of caveolins in cardiac muscle, this cardiac abnormality may be caused by secondary deficiency of caveolins in heart, as cardiac involvement was previously reported in patients with *CAV3* mutations and in mutant mice with double knockout of *Cav1* and *Cav3* (29–33).

Remarkable reduction in expression of caveolin-1 and -2 with decreased caveolae density was observed in vascular endothelial cells in P1–P5. There was no obvious symptom related to vascular endothelial blood vessels in the patients; however, further careful investigation is necessary in order to determine the involvement of endothelial cells, which was observed in *Cav1* knockout mice (34). The severe constipation and esophageal dilatation observed in the patients might be associated with dysfunction of caveolin-1 in smooth muscle cells, as *Cav1* knockout mice had alteration of

smooth muscles and interstitial cells of Cajal, the pacemaker cells of the muscle layers of the gastrointestinal tract (35).

Caveolae was previously suggested to have a role in the internalization of growth hormone in vitro (36). The acromegaloid features, accelerated bone age, or abnormal growth hormone activity observed in 3 patients in the present study might be associated with reduced caveolae formation. Recurrent pneumonia and transient immunodeficiency observed in 2 patients were also noted, although the pathomechanisms are still unknown. Further detailed studies are needed to elucidate the roles of *PTRF*; however,

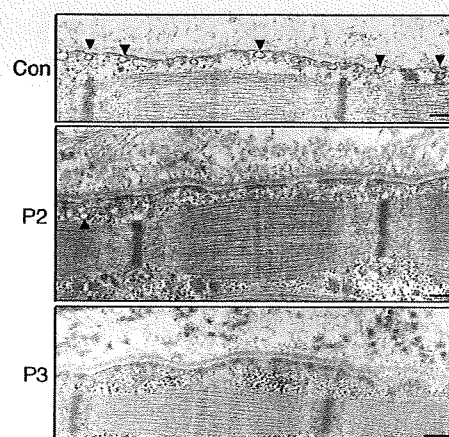


Figure 5 Reduced caveolae formation in skeletal muscle, as assessed by electron microscopy. In control muscle, an abundance of caveolae (arrowheads) was observed close to the plasma membrane. Plasma membrane of muscle fibers from P2 and P3 was nearly flat, and caveolae density was greatly reduced compared with that of control muscle. Only a few caveolae were seen in P2. Scale bars: 200 nm

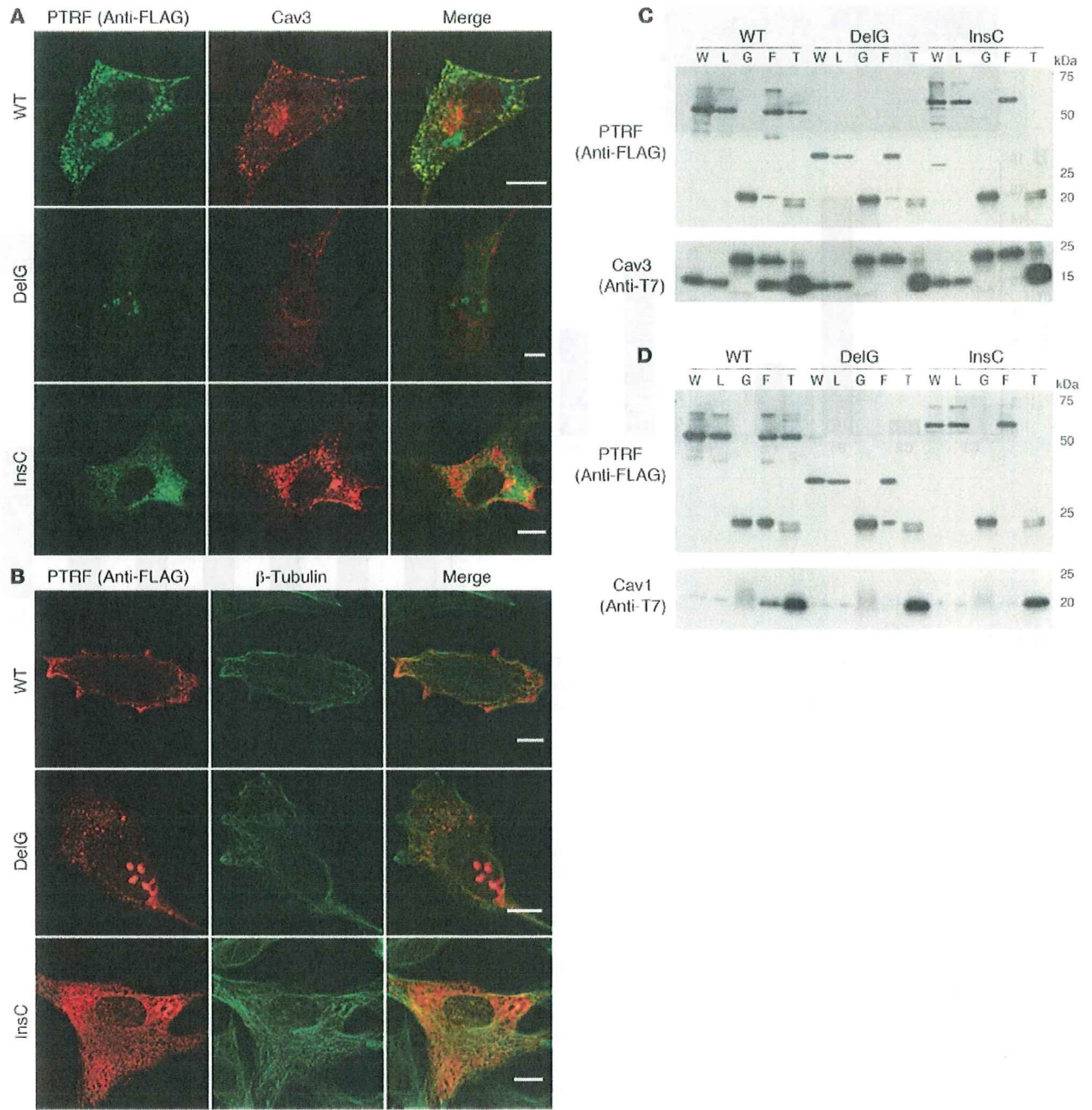


Figure 6

Altered localization of mutant PTRF in C2C12 cells and reduced binding ability to caveolins. C2C12 myoblasts were cotransfected with FLAG-tagged WT or mutant (c.525delG or c.696_697insC) PTRF cDNA and T7-tagged human caveolin-3. (A and B) WT PTRF stained by anti-FLAG antibody colocalized with caveolin-3 at the cell membrane. The deletion mutant accumulated in the nucleus, and the insertion mutant was seen in cytoplasm. (A) Membrane staining of caveolin-3 was decreased and was not colocalized with mutant PTRF. (B) The PTRF insertion mutant clearly colocalized with β -tubulin. Scale bars: 10 μ m. (C and D) COS-7 cells were cotransfected with FLAG-tagged WT or mutant PTRF cDNA and T7-tagged human caveolin-3 (C) or caveolin-1 (D). The PTRF deletion mutant showed smaller molecular weight (estimated 30 kDa), and no immunoprecipitated protein was detected for FLAG or T7 antibodies. The PTRF insertion mutant showed slightly larger molecular weight, and amounts of coimmunoprecipitated proteins were greatly reduced. W, whole homogenate; L, cell lysate; G, control IgG; F, anti-FLAG; T, anti-T7.

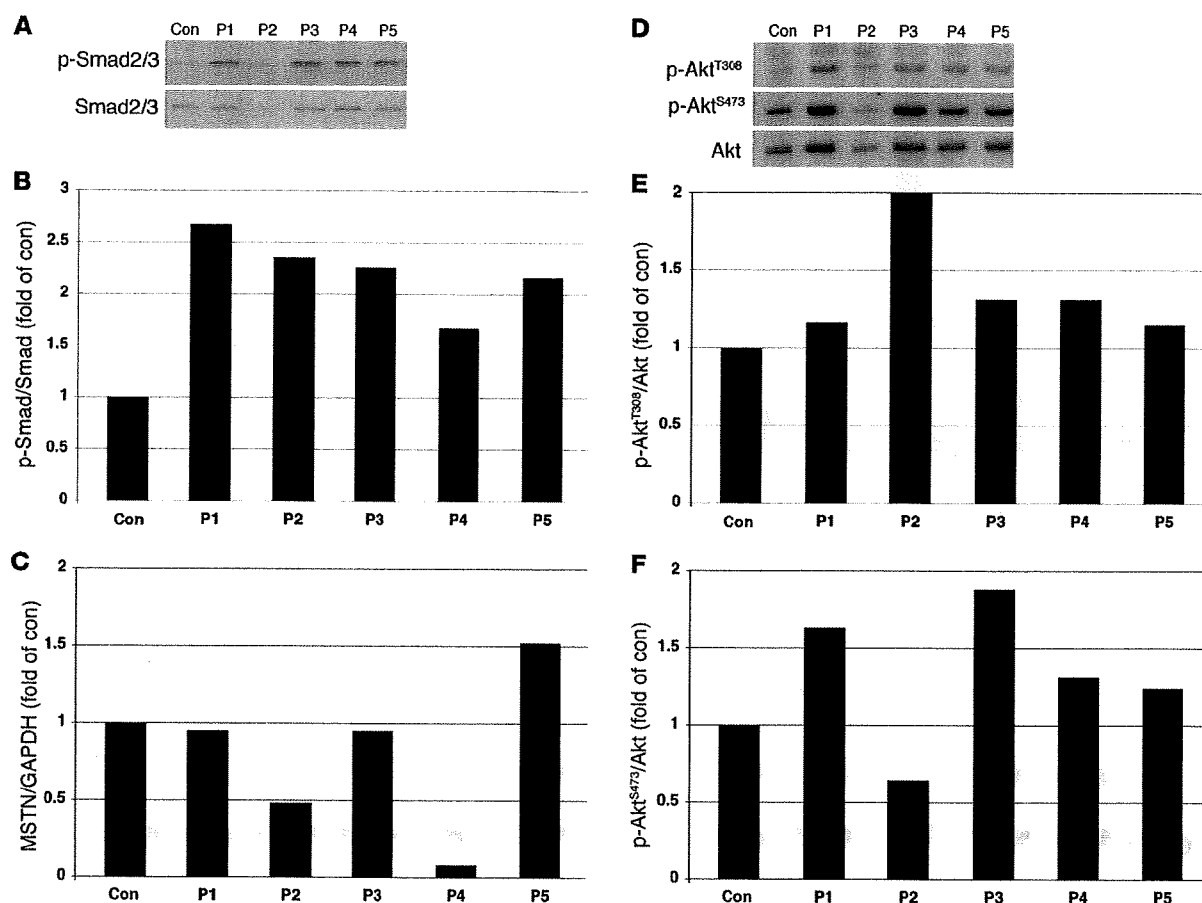


Figure 7

Increased p-Smad2 and p-Akt in P1–P5 skeletal muscle. (A–C) Immunoblotting analysis of Smad2/3 and p-Smad2/3^{S423/426} (A) and densitometric analysis (B) showed increased p-Smad2/3 in P1–P5 compared with control muscle, with variable mRNA expression levels of myostatin (MSTN; C). (D–F) Immunoblotting analysis of p-Akt^{T308} and p-Akt^{S473}. Total Akt (D) and densitometric analysis (E and F) showed increased amounts of p-Akt in all patients except for p-Akt^{S473} in P2.

most clinical features observed in P1–P5 are likely to be explained by secondary reduction of caveolae and deficiency of caveolins.

Previously, Rajab et al. reported 10 of 17 patients with congenital generalized lipodystrophy unlinked to the loci of known CGL genes (37). The patients showed reduced exercise tolerance, percussion myoedema, cardiac hypertrophy, and arrhythmias. None of these patients had insulin resistance or early endocrine abnormalities (37). Ghanem also reported myoedema in a patient with Berardinelli-Seip lipodystrophy (38). Very recently, Simha et al. described CGL patients with muscle weakness and cervical spine instability (39). Because muscle involvement of these patients is similar to that of P1–P5 in the present study, *PTRF* mutations may not be rare in CGL patients.

This entity of generalized lipodystrophy with muscular dystrophy – which we believe to be novel – seems to represent a complicated disorder, as the occurrence of other symptoms could not readily be explained. Collection of detailed clinical information would therefore be essential in order to understand the precise function of *PTRF*.

Methods

Clinical materials. All clinical materials used in this study were obtained for diagnostic purposes and with informed consent. Subjects were

selected from 2,745 muscular dystrophy specimens kept in the muscle repository of the National Center of Neurology and Psychiatry. The present studies were approved by the Ethical Committee at National Center of Neurology and Psychiatry.

Mutation screening and haplotype analysis. Genomic DNA was isolated from peripheral lymphocytes or muscles using standard techniques. All exons and their flanking intronic regions of *PTRF*, *CAV3*, *LMNA*, *AGPAT2*, *BSCL2*, *CAVI*, *PPARG*, *AKT2*, and *ZMPSTE24* were directly sequenced using genomic DNA from all patients using an ABI PRISM 3100 automated sequencer (Applied Biosystems). Primer sequences are listed in Supplemental Table 3. To confirm the compound heterozygosity in P5, the PCR product was cloned and sequenced. In order to determine the frequency of the mutations in *PTRF*, we performed enzyme digestion of PCR products from 200 Japanese control subjects using *Hpy188III* (New England Biolabs) for c.696_697insC and *TaqI* (New England Biolabs) for c.525delG. *MboII* (New England Biolabs) was used for enzyme digestion of PCR products to detect the c.1138G>A substitution in *BSCL2*.

For haplotype analysis, we used 6 SNPs (rs2062213, rs8070945, rs963988, rs963987, rs963986, and rs9252) within *PTRF*. PCR products were analyzed by direct sequencing or enzyme digestion using *MaeIII* (Boehringer Mannheim). We also identified a novel 9-bp insertion polymorphism at the

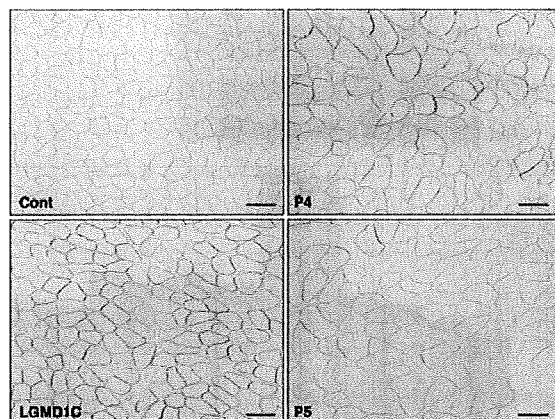


Figure 8
NDP activity assay. NDP activity was variable between muscle fibers, and was slightly increased in the muscle of P4, P5, and a LGMD1C patient with CAV3 mutation compared with an age-matched control subject. Scale bars: 100 μ m.

3' noncoding region, and its frequency was calculated by PCR amplification using 50 Japanese control individuals. We also examined 2 microsatellite markers, STS-W93348 and D17S1185, the closest markers to *PTRF*. PCR product size was analyzed by GeneMapper using ABI 310 automated sequencer (Applied Biosystems).

Histochemical analysis. Biopsied muscle specimens were flash frozen with isopentane cooled in liquid nitrogen. Serial 10- μ m-thick frozen sections were analyzed with 20 kinds of histochemical staining, including H&E, modified Gomori trichrome, NADH-tetrazolium reductase, and oil red O. The NDP activity assay was performed to examine nNOS activity of each muscle fiber, as described previously (40). In brief, 10- μ m-thick frozen sections were fixed with 4% paraformaldehyde in PBS for 2 hours at 4°C. After a brief rinse with PBS, sections were incubated with 0.2% Triton X-100 in PBS for 20 minutes at 37°C. The reaction was performed for 1 hour in a dark, humidified chamber at 37°C in 0.2% Triton X-100, 0.2 mM NADPH, and 0.16 mg/ml nitro blue tetrazolium. The reaction was terminated by washing with water. We examined 6 age-matched controls and 2 LGMD1C patients with CAV3 mutations (p.R27G and p.E33K).

Immunohistochemical analysis. Immunostaining was performed using standard methods. Serial 6- μ m-thick frozen muscle sections were fixed in cold acetone for 5 minutes. After blocking with normal goat serum, sections were incubated with the primary antibodies for 2 hours at 37°C. We used antibodies against PTRF (A301-269A and A301-271A; BETHYL Laboratories), caveolin-1 (BD Biosciences), caveolin-2 (Sigma-Aldrich), caveolin-3 (BD Biosciences), and nNOS (BD Biosciences). Rabbit anti-PTRF antibody of A301-269A recognizes residue from 125 to 175, and A301-271A was raised against residue 238 and 288 of human PTRF (Figure 1B). In order to exclude other diagnosable muscular dystrophies, we used antibodies for dystrophin (DYS1, DYS2, and DYS3; Novocastra); α -, β -, γ -, and δ -sarcoglycans (Novocastra); α -dystroglycan (Upstate Biotech); β -dystroglycan (Novocastra); dysferlin (Novocastra); emerin (Novocastra); merosin (Chemicon); and collagen VI (ICN Biomedicals). After 6 rinses with PBS, sections were incubated with secondary antibodies of Alexa Fluor 488 or Alexa Fluor 568 labeled goat anti-mouse or rabbit antibodies at room temperature for 45 minutes.

Immunoblotting analysis. Immunoblotting analysis was performed according to standard methods. Frozen muscle specimens were homogenized in SDS sample buffer and centrifuged at 15,000 g for 5 minutes. Protein (20 μ g) from each sample was loaded on 12% SDS-polyacrylamide gels and transferred to

PVDF membranes (Millipore). The membranes were blocked with 5% skim milk in PBS and immunoreacted with antibodies to PTRF (A301-269A and A301-271A), caveolin-2, caveolin-3, nNOS, Smad2/3 (Cell Signaling Technology), p-Smad2/3^{S423/S425} (Santa Cruz Biotechnology Inc.), Akt (Cell Signaling Technology), p-Akt^{T308} (Cell Signaling Technology), and p-Akt^{S473} (Cell Signaling Technology) overnight at 4°C. After washing in PBS containing 0.1% Tween-20, the membrane was incubated with horseradish peroxidase-labeled secondary antibody and visualized with ECL (Amersham Pharmacia Biotech). Data were analyzed using LAS-1000 chemiluminescence imaging system (Fujifilm). Quantification of immunoreactive bands was performed by densitometric analysis using Quantity One (PDI), and protein amounts for caveolin-3 and nNOS were normalized by the intensity of MHC. The ratio of p-Smad2/3 and p-Akt, to Smad and Akt, respectively, was also calculated.

Electron microscopy. Muscle specimens were fixed with 2% glutaraldehyde in 0.1 M cacodylate buffer. After shaking with a mixture of 4% osmium tetroxide, 1.5% lanthanum nitrate, and 0.2 M *s*-collidine for 2–3 hours, samples were embedded in epoxy resin. Semithin sections (1 μ m thick) were stained with toluidine blue. Ultrathin sections 50 nm thick were stained with uranyl acetate and lead citrate, then examined under H-600 transmission electron microscope (Hitachi) at 75 kV.

RT-PCR. Total RNA was extracted from biopsied skeletal muscles using TRIzol (Invitrogen), and RT-PCR was performed using SuperScript III (Invitrogen) with random hexamer according to the manufacturer's instructions. Primers for each gene were located on different exons or directly spanning exon-exon boundaries of the genomic sequence in order to minimize amplification from any contaminating genomic DNA. After performing preliminary gradient PCR assays, the optimal annealing temperature for all the primer pairs was determined in order to generate the lowest Ct value as well as a sharp melting peak, with no amplification of nonspecific products or primer-dimer artifacts. Quantitative RT-PCR was performed to compare the mRNA expression of caveolin-1, caveolin-2, caveolin-3, and myostatin using Rotor-Gene 6000 according to the manufacturer's instructions (Corbett Life Science). The reactions were performed in reference to the GAPDH. We used 4 points consisting of 10-fold serial dilution using each primer set to build the standard curve. The PCR reaction (50 cycles) was followed by a melting curve analysis, ranging from 72°C to 95°C, with temperature increasing steps of 0.5°C every 10 seconds. Baseline and threshold values were automatically determined and analyzed. R^2 values exceeded 0.97. The 2-standard curve method was used to determine the relative expression ratio of the target gene in the patient samples versus the control sample, with reference to GAPDH expression.

Cell culture and transfection. COS-7 and C2C12 cells were maintained at 37°C in a humidified atmosphere of 5% CO₂ in DMEM (Sigma-Aldrich) supplemented with 10% fetal bovine serum. Full-length PTRF and caveolin-1 and -3 were amplified using total RNA from control human muscle and cloned into the pGEM-T-easy vector (Promega). The PTRF mutants c.525delG and c.696_697insC were generated using appropriate primers. All primer sequences are shown in Supplemental Table 3.

Immunocytochemistry. COS-7 and C2C12 myoblasts were cotransfected with FLAG-tagged WT or mutant (c.525delG or c.696_697insC) PTRF cDNA and T7-tagged human caveolin-3 using FuGENE6 (Roche). Transfectants were fixed for 30 minutes in 2% paraformaldehyde or 100% methanol, then permeabilized in 0.1% Triton X-100 for 10 minutes. Polyclonal antibodies to FLAG (Sigma-Aldrich) with caveolin-3 (BD Biosciences) or FLAG with β -tubulin (Calbiochem) were applied for double staining.

Immunoprecipitation. COS-7 cells were cotransfected with FLAG-tagged WT or mutant (c.525delG or c.696_697insC) PTRF cDNA and T7-tagged human caveolin-1 or caveolin-3 using FuGENE6 (Roche). The sequences of all constructs were verified with DNA sequencing using ABI PRISM 310 (Applied Biosystems). After 48 hours, the lysates from transfectants were

solubilized with 50 mM Tris-HCl (pH 7.5), 150 mM NaCl, 50 mM EDTA, 1% Triton X-100, and Complete-mini EDTA-free proteinase inhibitors (Roche) (9). The solubilized lysate precleared with Protein G Sepharose (GE Healthcare) was incubated with anti-FLAG (M2; Sigma-Aldrich) and anti-T7 (Novagen) antibodies. Immunoprecipitated proteins were dissociated from beads by boiling in sample buffer and were resolved by SDS-PAGE. Immunoblotting was performed using standard techniques.

Acknowledgments

We thank Sherine Shalaby (Heliopolis Neurocenter, Cairo, Egypt) and May Malicdan (National Center of Neurology and Psychiatry) for reviewing the manuscript. This study was supported by "Research on Psychiatric and Neurological Diseases and Mental Health" of "Health Labour Sciences Research Grant" and by "Research Grant (20B-12, 20B-13) for Nervous and Mental Disorders" from the Ministry of Health, Labor, and Welfare

of Japan; by grants from the Human Frontier Science Program; by a Grant-in-Aid for Scientific Research from Japan Society for the Promotion of Science; by Research on Publicly Essential Drugs and Medical Devices from the Japanese Health Sciences Foundation; and by the Program for Promotion of Fundamental Studies in Health Sciences of the National Institute of Biomedical Innovation (NIBIO).

Received for publication January 20, 2009, and accepted in revised form June 3, 2009.

Address correspondence to: Yukiko K. Hayashi, Department of Neuromuscular Research, National Institute of Neuroscience, National Center of Neurology and Psychiatry, 4-1-1 Ogawahigashi, Kodaira, 187-8502 Tokyo, Japan. Phone: 81-42-341-2711, Fax: 81-42-346-1742; E-mail: hayasi_y@ncnp.go.jp.

- Scherer, P.E., et al. 1997. Cell-type and tissue-specific expression of caveolin-2. Caveolins 1 and 2 co-localize and form a stable hetero-oligomeric complex in vivo. *J. Biol. Chem.* **272**:29337-29346.
- Tang, Z., et al. 1996. Molecular cloning of caveolin-3, a novel member of the caveolin gene family expressed predominantly in muscle. *J. Biol. Chem.* **271**:2255-2261.
- Galbiati, F., Razani, B., and Lisanti, M.P. 2001. Emerging themes in lipid rafts and caveolae. *Cell* **106**:403-411.
- Thomas, C.M., and Smart, E.J. 2008. Caveolae structure and function. *J. Cell. Mol. Med.* **12**:796-809.
- Hill, M.M., et al. 2008. PTRF-Cavin, a conserved cytoplasmic protein required for caveola formation and function. *Cell* **132**:113-124.
- Liu, L., et al. 2008. Deletion of Cavin/PTRF causes global loss of caveolae, dyslipidemia, and glucose intolerance. *Cell Metab.* **8**:310-317.
- Minetti, C., et al. 1998. Mutations in the caveolin-3 gene cause autosomal dominant limb-girdle muscular dystrophy. *Nat. Genet.* **18**:365-368.
- Matsuda, C., et al. 2001. The sarcolemmal proteins dysferlin and caveolin-3 interact in skeletal muscle. *Hum. Mol. Genet.* **10**:1761-1766.
- Liu, L., and Pilch, P.F. 2008. A critical role of cavin (polymerase I and transcript release factor) in caveolae formation and organization. *J. Biol. Chem.* **283**:4314-4322.
- Minetti, C., et al. 2002. Impairment of caveolae formation and T-system disorganization in human muscular dystrophy with caveolin-3 deficiency. *Am. J. Pathol.* **160**:265-270.
- Ohsawa, Y., et al. 2006. Muscular atrophy of caveolin-3-deficient mice is rescued by myostatin inhibition. *J. Clin. Invest.* **116**:2924-2934.
- Frost, R.A., and Lang, C.H. 2007. Protein kinase B/Akt: a nexus of growth factor and cytokine signaling in determining muscle mass. *J. Appl. Physiol.* **103**:378-387.
- Venema, V.J., Ju, H., Zou, R., and Venema, R.C. 1997. Interaction of neuronal nitric-oxide synthase with caveolin-3 in skeletal muscle. Identification of a novel caveolin scaffolding/inhibitory domain. *J. Biol. Chem.* **272**:28187-28190.
- Sunada, Y., et al. 2001. Transgenic mice expressing mutant caveolin-3 show severe myopathy associated with increased nNOS activity. *Hum. Mol. Genet.* **10**:173-178.
- Agarwal, A.K., et al. 2002. AGPAT2 is mutated in congenital generalized lipodystrophy linked to chromosome 9q34. *Nat. Genet.* **31**:21-23.
- Magre, J., et al. 2001. Identification of the gene altered in Berardinelli-Seip congenital lipodystrophy on chromosome 11q13. *Nat. Genet.* **28**:365-370.
- Kim, C.A., et al. 2008. Association of a homozygous nonsense caveolin-1 mutation with Berardinelli-Seip congenital lipodystrophy. *J. Clin. Endocrinol. Metab.* **93**:1129-1134.
- Cao, H., Alston, L., Ruschman, J., and Hegele, R.A. 2008. Heterozygous CAV1 frameshift mutations (MIM 601047) in patients with atypical partial lipodystrophy and hypertriglyceridemia. *Lipids Health Dis.* **7**:3.
- Cao, H., and Hegele, R.A. 2000. Nuclear lamin A/C R482Q mutation in Canadian kindreds with Dunnigan-type familial partial lipodystrophy. *Hum. Mol. Genet.* **9**:109-112.
- Agarwal, A.K., et al. 2003. Phenotypic and genetic heterogeneity in congenital generalized lipodystrophy. *J. Clin. Endocrinol. Metab.* **88**:4840-4847.
- George, S., et al. 2004. A family with severe insulin resistance and diabetes due to a mutation in AKT2. *Science* **304**:1325-1328.
- Barroso, L., et al. 1999. Dominant negative mutations in human PPARgamma associated with severe insulin resistance, diabetes mellitus and hypertension. *Nature* **402**:880-883.
- Hegele, R.A., et al. 2006. Sequencing of the reannotated LMNB2 gene reveals novel mutations in patients with acquired partial lipodystrophy. *Am. J. Hum. Genet.* **79**:383-389.
- Aboulaich, N., Ortegren, U., Vener, A.V., and Stralfors, P. 2006. Association and insulin regulated translocation of hormone-sensitive lipase with PTRF. *Biochem. Biophys. Res. Commun.* **350**:657-661.
- Razani, B., et al. 2002. Caveolin-1-deficient mice are lean, resistant to diet-induced obesity, and show hypertriglyceridemia with adipocyte abnormalities. *J. Biol. Chem.* **277**:8635-8647.
- Fulizio, L., et al. 2005. Molecular and muscle pathology in a series of caveolinopathy patients. *Hum. Mutat.* **25**:82-89.
- Berz, R.C., et al. 2001. Mutations in CAV3 cause mechanical hyperirritability of skeletal muscle in rippling muscle disease. *Nat. Genet.* **28**:218-219.
- Sugie, K., et al. 2004. Two novel CAV3 gene mutations in Japanese families. *Neuromuscul. Disord.* **14**:810-814.
- Hayashi, T., et al. 2004. Identification and functional analysis of a caveolin-3 mutation associated with familial hypertrophic cardiomyopathy. *Biochem. Biophys. Res. Commun.* **313**:178-184.
- Varra, M., et al. 2006. Mutant caveolin-3 induces persistent late sodium current and is associated with long-QT syndrome. *Circulation* **114**:2104-2112.
- Park, D.S., et al. 2002. Caveolin-1/3 double-knockout mice are viable, but lack both muscle and non-muscle caveolae, and develop a severe cardiomyopathic phenotype. *Am. J. Pathol.* **160**:2207-2217.
- Woodman, S.E., et al. 2002. Caveolin-3 knockout mice develop a progressive cardiomyopathy and show hyperactivation of the p42/44 MAPK cascade. *J. Biol. Chem.* **277**:38988-38997.
- Zhao, Y.Y., et al. 2002. Defects in caveolin-1 cause dilated cardiomyopathy and pulmonary hypertension in knockout mice. *Proc. Natl. Acad. Sci. U. S. A.* **99**:11375-11380.
- Xu, Y., Buikema, H., van Gilst, W.H., and Henning, R.H. 2008. Caveolae and endothelial dysfunction: filling the caves in cardiovascular disease. *Eur. J. Pharmacol.* **585**:256-260.
- El-Yazbi, A.F., Cho, W.J., Boddy, G., and Daniel, E.E. 2005. Caveolin-1 gene knockout impairs nitric oxide function in mouse small intestine. *Br. J. Pharmacol.* **145**:1017-1026.
- Lobie, P.E., Sadir, R., Graichen, R., Meitani, H.C., and Morel, G. 1999. Caveolar internalization of growth hormone. *Exp. Cell Res.* **246**:47-55.
- Rajab, A., Heathcote, K., Joshi, S., Jeffery, S., and Patron, M. 2002. Heterogeneity for congenital generalized lipodystrophy in seventeen patients from Oman. *Am. J. Med. Genet.* **110**:219-225.
- Ghanem, Q. 1993. Percussion myoedema in a Pakistani boy with Berardinelli-Seip lipodystrophy syndrome. *Clin. Genet.* **44**:277-278.
- Simha, V., Agarwal, A.K., Aronin, P.A., Iannaccone, S.T., and Garg, A. 2008. Novel subtype of congenital generalized lipodystrophy associated with muscular weakness and cervical spine instability. *Am. J. Med. Genet. A.* **146A**:2318-2326.
- Kameya, S., et al. 1999. alpha1-syntrophin gene disruption results in the absence of neuronal-type nitric oxide synthase at the sarcolemma but does not induce muscle degeneration. *J. Biol. Chem.* **274**:2193-2200.

